Characterization and Catalytic Functionalities of Copper Oxide Catalysts Supported on Zirconia

ARTICLE *in* THE JOURNAL OF PHYSICAL CHEMISTRY B · FEBRUARY 2007

Impact Factor: 3.3 · DOI: 10.1021/jp063335x · Source: PubMed

4 AUTHORS, INCLUDING:

Vidya Sagar Guggilla
Reliance Industries Limited
19 PUBLICATIONS **466** CITATIONS
SEE PROFILE

Srikanth Chakravartula Srivatsa
Monash University (Australia)
16 PUBLICATIONS **235** CITATIONS
SEE PROFILE

Characterization and Catalytic Functionalities of Copper Oxide Catalysts Supported on Zirconia

Komandur V. R. Chary,* Guggilla Vidya Sagar, Chakravarthula S. Srikanth, and Vattikonda Venkat Rao

Catalysis Division, Indian Institute of Chemical Technology, Hyderabad − 500 007, India

Received: May 30, 2006; In Final Form: August 23, 2006

A series of zirconia supported copper oxide catalysts with varying copper loadings (1.2−19.1 wt %) were prepared by impregnation method. The catalysts were characterized by X-ray diffraction, UV−visible diffuse reflectance spectroscopy, X-ray photoelectron spectroscopy (XPS), temperature-programmed reduction (TPR), and temperature-programmed desorption of CO_2. Copper dispersion and metal area were determined by N_2O decomposition method. X-ray diffraction patterns indicate the presence of crystalline CuO phase beyond 2.7 wt % of Cu on zirconia. UV−visible diffuse reflectance spectra suggest the presence of two types of copper species on the ZrO_2 support. XPS peaks intensity ratio of Cu $2p_{3/2}$ and Zr $3d_{5/2}$ was compared with Cu dispersion calculated from N_2O decomposition. TPR patterns reveal the presence of highly dispersed copper oxide at lower temperatures and bulk CuO at higher temperatures. The basicity of the catalysts was found to increase with Cu loading, and the activity of the catalysts was also found to increase with the increase in Cu loading up to 2.7 wt % Cu loading. The catalytic properties were evaluated for the dehydrogenation of cyclohexanol to cyclohexanone and were related to surface properties of the copper species supported on zirconia.

1. Introduction

Catalysts with copper oxide as an active component have been extensively employed in the recent past for the selective catalytic reduction of NO_x and synthesis and steam reforming of methanol.[1−5] Copper catalysts are very selective in hydrogenation−dehydrogenation reactions such as conversion of benzaldehyde to benzyl alcohol,[6] furfural to furfuryl alcohol,[7] or the transformation of alcohols into their corresponding aldehydes or ketones.[8−10] The catalytic properties of the active copper oxide phase can be greatly influenced by the nature of the supported oxide and the dispersion of active component. Zirconia based materials have attracted considerable interest in recent years for their potential use as catalyst supports.[3,11−14] ZrO_2 presents special characteristics such as high thermal stability, extreme hardness, and stability under reducing conditions. Further the possession of both acid and base functions make it very appealing as a carrier for several catalytic applications.[14] In the catalytic sense, these have some advantages over traditional catalyst supports, such as SiO_2 and Al_2O_3,[15] in the areas of practical application. Zirconia is often included in heterogeneous systems, either as a promoter or more generally as a support. In CO hydrogenation for instance, zirconia addition to metal supported catalysts induces a long-term stability[16,17] and also enhances both the activity[18−20] and the selectivity towards alcohol.[21,22] It has also been employed in many industrially important reactions such as hydroprocessing,[23] oxidation of alcohols,[24−26] dehydrogenation of cyclohexanol,[27] and synthesis of methanol and higher alcohols.[28] Amenomiya[29] reported that the catalytic activity of CuO/ZrO_2 is better than those of CuO/Al_2O_3, CuO/SiO_2, CuO/MgO, and CuO/TiO_2 catalytic systems for the methanol synthesis from hydrogenation of CO_2. Takezawa et al.[30] revealed that the catalytic activity of copper oxide supported on zirconia for the steam reforming of methanol was improved when compared to Cu/SiO_2.

The study of determination of dispersion of the active phase in supported Cu catalysts is an interesting topic of research in recent years for understanding the nature of active phase on the catalytic properties. A fundamental understanding of the structure−activity relationship in heterogeneous catalytic dehydrogenation is of basic importance for the development of new catalytic materials and for improving the performance of existing catalysts. For this, N_2O decomposition was chosen to find active phase dispersion in supported copper catalysts.[31]

In the present investigation we report the characterization of CuO/ZrO_2 catalysts by powder X-ray diffraction (XRD), UV−vis diffuse reflectance spectroscopy (UV−DRS), X-ray photoelectron spectroscopy (XPS), temperature-programmed reduction (TPR), and temperature-programmed desorption (TPD) of CO_2. Cu dispersion and metal area were determined by N_2O decomposition. The catalytic properties were evaluated for the vapor phase dehydrogenation of cyclohexanol to cyclohexanone. The purpose of this work is to estimate the dispersion of CuO supported on zirconia as a function of copper loading, in order to identify changes in the structure of the CuO phase with loading to understand the relation between the dispersion of Cu and basicity of catalyst for dehydrogenation of cyclohexanol and also to compare with other supported copper catalysts.

2. Experimental Section

Zirconia support was prepared from saturated aqueous zirconyl nitrate hydrate $ZrO(NO_3)_2 \cdot xH_2O$ (Fluka), with the addition of aqueous ammonia till pH reaches to 9. The resulting precipitate was washed repeatedly with portions of deionized water until the precipitate is free from the base. The precipitate was dried at 383 K for 12 h, and the resulting hydroxide was calcined in air at 773 K for 5 h. A series of copper catalysts

* Corresponding author. Fax: +91-40-27160921. Tel: +91-40-27193162. E-mail: kvrchary@iict.res.in.

10.1021/jp063335x CCC: $37.00
Published on Web 12/29/2006

with Cu loadings varying from 1.2 to 19.1 wt % were prepared by impregnation with requisite amount of Cu $(NO_3)_2 \cdot 3H_2O$ (Fluka) on ZrO_2 support. The samples were dried at 383 K for 16 h and subsequently calcined at 773 K for 5 h in air. The same set of catalysts were used for all characterization and evaluation studies.

The copper content was determined by atomic absorption spectroscopy using a Perkin-Elmer Analyst 300 double beam spectrometer. The powders were first dissolved in acidic solution (40% HF) and diluted to concentrations within the detection range of the instrument.

X-ray powder diffraction patterns were obtained with a Siemens D5000 diffractometer, using Cu Kα radiation (1.5406 Å) at 40 kV and 30 mA and a secondary graphite monochromator. The measurements were recorded in steps of 0.045° with a count time of 0.5 s in the 2θ range of 2−65°.

The specific surface areas of the catalyst samples were calculated from N_2 adsorption−desorption data acquired on a single point Pulse Chemisorb 2700 instrument (Micromeritics, USA) at liquid N_2 temperature. The powders were first outgassed at 423 K to ensure a clean surface prior to construction of adsorption isotherm. A cross-sectional area of 0.164 nm^2 of the N_2 molecule was assumed in the calculations of the specific surface areas using the method of Brunauer, Emmet, and Teller (BET). Pore size distribution (PSD) measurements were performed on Auto Pore III (Micromeritics) by mercury penetration method.

UV−visible spectra were recorded in air at room temperature using a GBC UV−visible Cintra 10_e spectrometer with a diffuse reflectance accessory, in the 200−900 nm wavelength range. The ZrO_2 support was used as reference. The Kubelka−Munk function $F(R)$ was plotted against the wavelength (in nm).

X-ray photoelectron spectroscopy was used to study the chemical composition and oxidation state of catalyst surfaces. The XPS spectra of the catalysts were measured on a XPS spectrometer (Kratos-Axis 165) with Mg Kα radiation ($h\nu$ =1253.6 eV) at 75 W. The Cu 2p and Zr 3d core-level spectra were recorded and the corresponding binding energies were referenced to the C 1s line at 284.6 eV (accuracy within ±0.2 eV). The background pressure during the data acquisition was kept below 10^{-10} bar.

Temperature-programmed reduction studies were carried out on a Auto Chem 2910 (Micromeritics, USA) instrument to study the copper dispersion and reducibility. In a typical experiment, Ca. 250 mg of oven-dried sample (dried at 383 K for 15 h) was taken in a U-shaped quartz sample tube. The catalyst was mounted on a quartz wool plug. Prior to TPR studies, argon gas was passed with a flow of 50 mL/min at 393 K for 2 h to pretreat the catalyst sample. After pretreatment, the sample was cooled to ambient temperature and TPR analysis was carried out in a flow of 5% H_2−Ar mixture (50 mL/min) from ambient temperature to 673 K at a heating rate of 10 K/min. H_2 consumption and T_{max} positions are calculated using GRAMS/32 software.

Temperature-programmed desorption (TPD) studies were also conducted on same instrument. In a typical experiment for TPD studies ca. 200 mg of oven dried sample (dried at 383 K for overnight) was taken in an U-shaped quartz sample tube. Prior to TPD studies, the catalyst sample was pretreated at 473 K for 30 min by passing very pure helium (99.999%, 50 mL/min). After pretreatment of the sample, it was reduced at 523 K for 2 h by passing very pure hydrogen (99.99%, 50 mL/min) and subsequently flushed with pure helium (50 mL/min) for 30 min to ensure a clean surface. After reducing the sample, it was saturated with CO_2 in a flow of 10% CO_2−He mixture at 303 K with a flow rate of 50 mL/min and was subsequently flushed at 378 K for 1 h to remove physisorbed CO_2. TPD analysis was carried out from ambient temperature to 1073 K at a heating rate of 10 K/min. The amount of CO_2 desorbed was also calculated using GRAMS/32 software.

Copper surface area, dispersion, and crystallite size were calculated by N_2O decomposition method conducted on a Auto Chem 2910 (Micromeritics, USA). This method consists of two steps (i) oxidation of Cu^0 to Cu_2O by N_2O and (ii) H_2 temperature-programmed-reduction of the formed Cu_2O surface species (s-TPR).[22] Before analysis, in-situ prereduction of the CuO phase to Cu^0 was performed in flow mixture of 5% H_2−Ar raising the temperature at a heating rate of 10 K/min up to 623 K. The catalyst was purged and cooled to 333 K in Ar and Cu^0 to Cu_2O oxidation was performed by adsorptive decomposition of N_2O at 333 K flowing N_2O (50 mL/min) for 45 min. In sequence, the catalyst was again purged in Ar flow and cooled to ambient temperature. After this, s-TPR was carried out similarly as in TPR, raising the temperature up to 723 K on the freshly oxidized Cu_2O surface in order to reduce Cu_2O to Cu^0. H_2 uptake was calculated using same GRAMS/32 software.

A down flow fixed bed reactor made of Pyrex glass was used to test the catalysts for the dehydrogenation of cyclohexanol to cyclohexanone at atmospheric pressure. About 500 mg of the catalyst diluted with an equal amount of quartz grains was charged into the reactor and was supported on a quartz wool bed. Prior to introducing cyclohexanol with a syringe pump, the catalyst was reduced at 523 K for 3 h, in purified hydrogen flow. After prereduction, the reactor was fed with cyclohexanol (6 mL/h) at 523 K in N_2 (flow rate 50 mL/min), which is used as a carrier gas. The liquid products, mainly cyclohexanone and cyclohexene, were analyzed by a Hewlett-Packard 6890 gas chromatograph equipped with a flame ionization detector using a HP-5 capillary column. The products were also identified using a HP 5973 quadrupole GC-MSD system using a HP-1MS capillary column.

3. Results and Discussion

The X-ray diffraction patterns of pure ZrO_2 and calcined CuO/ZrO_2 catalysts are shown in Figure 1. ZrO_2 exists in three crystallographic polymorphs viz., monoclinic, tetragonal, and cubic.[32] The zirconia synthesized in the present study shows the presence of mixed phases of monoclinic and tetragonal (Figure 1). In all the samples, XRD peaks due to ZrO_2 were observed at d = 3.676, 3.16, 2.842, and 1.65 Å (2θ = 24.2, 28.2, 31.5, and 55.65°) which are due to the monoclinic phase of zirconia and the peaks at d = 2.96, 2.60, 2.54, and 1.81 Å (2θ = 30.16, 34.46, 35.30, and 50.37°) are corresponding to tetragonal zirconia. At higher Cu loadings (above 2.7 wt % Cu, Figure 1), XRD peaks due to the crystalline CuO phase are noticed at d = 2.52 Å (2θ = 35.5°) and 2.38 Å (2θ = 38.7°), in addition to the characteristic peaks of zirconia. The intensity of these peaks were found to increase with Cu loading. However, at low Cu loadings the absence of crystalline CuO peaks cannot be ruled out as they might be less than 40 Å in size, which is beyond the detection capacity of the XRD technique. XRD results also suggest that no new crystalline oxide phase formation between CuO and ZrO_2. Normally, the monoclinic phase is stable below 1273 K and the tetragonal phase of ZrO_2 appears above 1400 K. Rijnten[33] and Afanaiev et al.[34] observed the tetragonal to monoclinic phase transformation occurs with the impregnation of molybdenum oxide. Maity et al.[35] have also observed phase transformation of zirconia in their study of

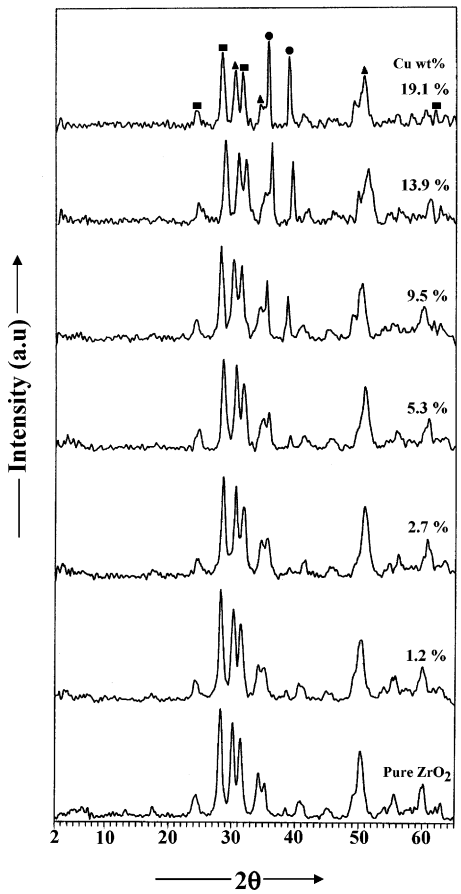

Figure 1. X-ray diffraction patterns of various CuO/ZrO_2 catalysts (■ due to monoclinic zirconia, ▲ due to tetragonal zirconia, ● due to CuO).

TABLE 1: BET Surface Area and Pore Size Distribution of Various CuO/ZrO_2 Catalysts

sample	wt % of Cu	BET surface area (m^2/g)	total pore volume (mL/g)	total pore area (m^2/ g)
1	0.0	74	0.37	74
2	1.2	54	0.32	63
3	2.7	55	–	–
4	5.3	51	0.27	57
5	9.5	49	–	–
6	13.9	47	0.25	53
7	19.1	45	–	–

zirconia supported hydrotreating catalysts. However, in the present study we did not observe any such phase transition after impregnation with copper nitrate when the samples were calcined at 773 K.

The BET surface area determined by nitrogen physisorption of all the catalysts are presented in Table 1. The specific surface area of the pure ZrO_2 support was found to be 74 m^2/g. The BET surface area decreases as a function of copper content on ZrO_2, and it might be due to surface hydroxyl groups (OH_{surf}) of the support consumed by reaction with the active phase precursor. Such a surface reaction may have caused the decrease of available surface area of the support, probably by closure of the pores as evidenced by PSD. Total pore volume and total pore area of samples measured by mercury penetrating porosimeter have also been reported in Table 1. The total pore volume and total pore area are found to decrease with increase of copper loading in the similar lines of surface area of the catalysts.

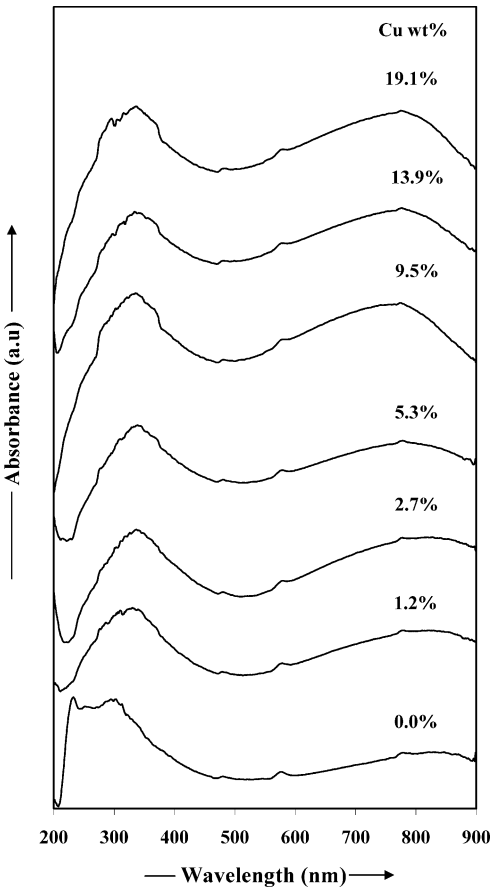

Figure 2. UV−visible diffuse reflectance spectra of various CuO/ZrO_2 catalysts.

The UV−visible spectra of calcined CuO/ZrO_2 samples are shown in Figure 2. For comparison, the diffuse reflectance (DR) spectrum of pure ZrO_2 sample was also recorded. The DR spectrum of pure ZrO_2 exhibits a characteristic band around 220 nm due to the $O_2^{2-} \rightarrow Zr^{4+}$ charge-transfer transition.[36] The DR spectrum of CuO/ZrO_2 catalysts show strong absorption bands at 350 nm and a large absorption band at 600−900 nm. The charge-transfer (CT) bands give an idea of the environment in the neighborhood of Cu^{2+} ions. According to earlier reports,[37,38] the band at 350 nm indicates the ligand-to-metal charge-transfer (LMCT) transition ($O^{2-} \rightarrow Cu^{2+}$), where the Cu ions occupy isolated sites over the support. The large absorption band at 600−900 nm is assigned to $^2E_g \rightarrow {}^2T_{2g}$ transitions of Cu^{2+} situated in more or less tetragonally distorted octahedral environment with an distorted O_h symmetry.[37] Iwamoto and his group[39] have reported that the peaks at 320 and 440 nm in the DR spectra of Cu-ZSM-5 zeolites were identified as a $O^{2-} \rightarrow Cu^{2+}$ and $(Cu-O-Cu)^{2+}$, respectively. Mendes et al.[40] have observed that the broad absorption band between 600 and 900 nm and the band at 350 nm indicate the formation of copper clusters different from those of bulk CuO. The $O^{2-} \rightarrow Cu^{2+}$ charge-transfer band at 350 nm is shifted to higher wavelength range and an increase in intensity of the broad absorption band between 600 and 900 nm is found with an increase of Cu loading. It clearly suggests the increase in crystallinity and formation of bulk CuO at higher loadings. This is also in good agreement with XRD results observed wherein the intensities of the CuO peaks increased with the increase of Cu loading.

The catalyst surface composition and oxidation state were investigated by XPS. Figures 3 and 4 show Zr 3d and Cu 2p XPS of various CuO/ZrO_2 calcined catalysts, respectively. The

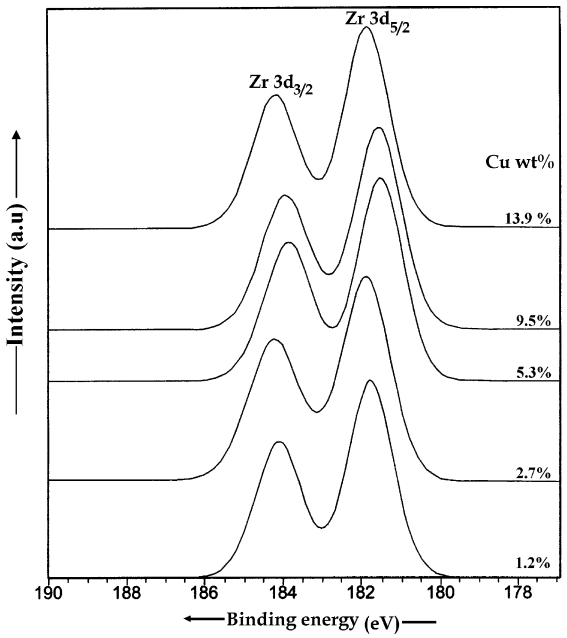

Figure 3. X-ray photoelectron spectra of Zr 3d spectra of various CuO/ZrO_2 catalysts.

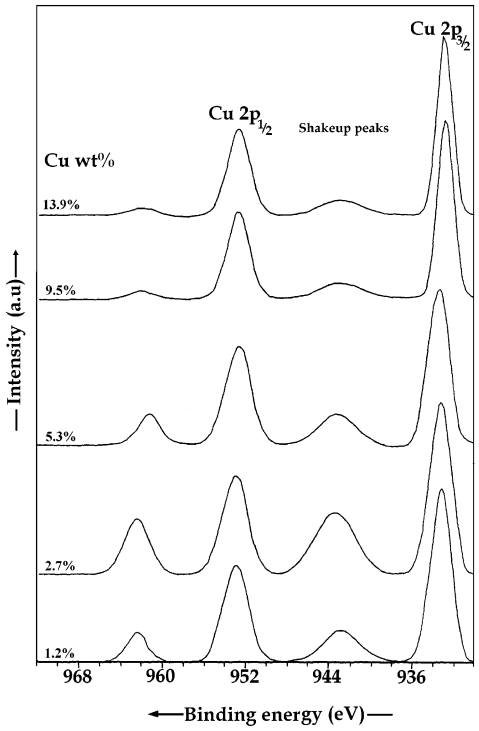

Figure 4. X-ray photoelectron spectra of Cu 2p spectra of various CuO/ZrO_2 catalysts.

$Zr\ 3d_{5/2}$ and $Zr\ 3d_{3/2}$ binding energy values are in the range of 181.8 and 184.5 eV, respectively. The binding energies of $Zr\ 3d_{5/2}$ and its full width at half maximum (FWHM) values are reported in Table 2. The constant FWHM values are found to be around 1.3, implying that only one type of doublet is present. This provides an evidence for the presence of a single type of zirconium oxide with an oxidation state of 4+. The intensity of Zr 3d core level spectra does not change much with increase of copper loading.

Figure 4 shows Cu 2p XPS of various CuO/ZrO_2 catalysts. The binding energy of the $Cu\ 2p_{3/2}$ peak at 934.2 eV together with FWHM of 3.8 eV and the characteristic shakeup feature at a binding energy of 944 eV are indicative for Cu^{2+} species.[41]

TABLE 2: XPS Results of Various CuO/ZrO_2 Catalysts

sample	Cu (wt %)	position and FWHM of Cu $2p_{3/2}$	position and FWHM of Zr $3d_{5/2}$	XPS intensity Cu 2p/Zr 3d
1	1.2	933.2 (1.9)	181.7 (1.35)	0.17
2	2.7	933.2 (2.3)	181.8 (1.33)	0.37
3	5.3	933.5 (1.9)	181.6 (1.33)	0.26
4	9.5	933.0 (1.7)	181.6 (1.35)	0.29
5	13.9	933.0 (1.7)	181.8 (1.38)	0.24

The binding energy and FWHM values of $Cu\ 2p_{3/2}$ peaks are listed in Table 2 for different copper loadings. Generally, the lower binding energy (932.2−933.1 eV) and absence of shakeup peaks are characteristics of Cu^{1+} ion.[42] The results indicate that copper species are present as Cu^{2+} in all the samples as indicated by shakeup peaks in Figure 4. The binding energy of the $Cu\ 2p_{3/2}$ transition for the various calcined CuO/ZrO_2 catalysts is found to be lower than the bulk CuO. Although CuO reduces readily to Cu_2O, the possibility of CuO reduction to Cu_2O cannot be ruled out during the XPS analysis.[43] The constant FWHM values are around 1.9, implying that only one type of doublet is present. This provides an evidence for the presence of a single type of copper oxide with an oxidation state of 2+. The intensity of Cu 2p core level spectra increases with the increase of Cu loading and levels off at higher loadings. This is also in good agreement with the previously reported XRD results, wherein the intensities of the CuO peaks increased with increase of Cu loading.

The XPS intensity ratio of Cu 2p/Zr 3d values for various CuO/ZrO_2 catalysts are reported in Table 2, which reflect the copper dispersion on zirconia support. The XPS intensity ratio of Cu 2p/Zr 3d increases with the increase of copper loading with a maxima at 2.7 wt % and then decreases with further increase of Cu loading. This could be probably due to the formation of large CuO crystallites. The XRD also further confirm detection of bulk CuO in the sample with 5.3 wt % and above copper loadings. The activity of the catalysts in the dehydrogenation of cyclohexanol to cyclohexanone was also found to increase up to 2.7 wt % Cu loading and decreases with further increase of Cu loading. A low dispersion of copper oxide is also noticed at higher Cu loadings on ZrO_2 by the N_2O decomposition method described later in this section. Thus, the present XPS results are in good agreement with the dispersion of copper determined by N_2O decomposition method.

Temperature-programmed reduction (TPR) has been extensively applied in recent years for characterizing reducible catalysts including metal and metal oxide systems. This technique, therefore, allows us to obtain a profile or 'finger print' of catalyst reduction. This is eminently suitable for studying low loading and highly dispersed systems whose characteristics are beyond the limits of detectability by other direct structural analysis methods (eg. X-ray diffraction). The TPR profiles of CuO/ZrO_2 catalysts are shown in Figure 5. All the samples exhibit two reduction profiles (α, β) during TPR in the temperature range of 454−567 K but for the samples containing low Cu loadings (1.2 and 2.7 wt %). The hydrogen consumption values and T_{max} during the TPR are reported in Table 3. The T_{max} position of α peak is shifting to the low-temperature region with increase of copper loading. When the copper loading is above 1.2 wt %, the α peak splits into two peaks (α_1, α_2). A β peak was observed at high-temperature region, when the copper loading is higher than 2.7 wt %, and its intensity is increased with increase of copper loading. The low-temperature TPR peak is attributed to the highly dispersed surface CuO species, and high-temperature TPR peak is attributed to the bulk CuO. Such

TABLE 3: Temperature-Programmed Reduction Results of Various CuO/ZrO_2 Catalysts

sample	Cu (wt %)	T_{max}^1 (K)	H_2 consumption^1 (μmol/g)	T_{max}^2 (K)	H_2 consumption^2 (μmol/g)	total H_2 consumption^{1+2} (μmol/g)
1	1.2	454	96	–	–	96
2	2.7	450	315	–	–	315
3	5.3	448	310	531	363	673
4	9.5	442	258	538	1217	1475
5	13.9	435	236	543	2039	2275
6	19.1	436	207	567	2837	3044

a low-temperature peak of TPR was also noticed by Shimokawabe et al.[44] and Dow et al.[45] They have reported that the low-temperature peaks were due to highly dispersed CuO with an octahedral environment of Cu^{2+} ions. Robertson et al.[46] and Vander Grift et al.[47] have also investigated the reduction behavior of CuO/SiO_2 catalysts and concluded that the highly dispersed copper oxide species were easily reducible when compared to bulk CuO. An explanation for the supported copper species for its easier reduction over the reference sample (bulk CuO) could be a dispersion effect, but it could also be an effect of interaction between the support and the copper species.[48,49] The highly dispersed copper species include both isolated Cu^{2+} ions that strongly and weakly interact with the support (the cupric ions have close contact with each other) and also a small two-dimensional clusters. The TPR peak at higher temperatures is attributed to large three-dimensional clusters. As the loading increases, the TPR peak becomes broad and shifts to high temperature. The broadening of the peak and shifting of the T_{max} toward higher temperatures might be due to increase in crystallinity of CuO with increase of Cu loading as evidenced from XRD results. As can be seen from Table 3, the H_2 consumption of the α peak is found to be the highest for 2.7 wt % of Cu loading among all the samples. This clearly suggests

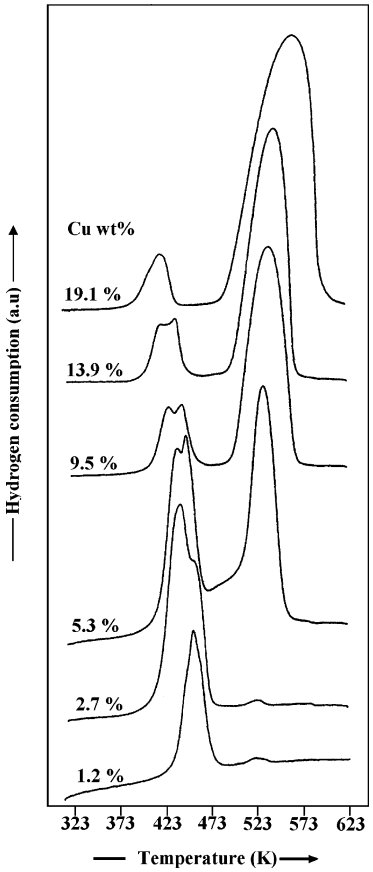

Figure 5. Temperature-programmed reduction profiles of various CuO/ZrO_2 catalysts.

TABLE 4: Dispersion, Copper Metal Area, and Average Particle Size of Various CuO/ZrO_2 Catalysts

sample	Cu (wt %)	dispersion (%)	Cu metal area (m^2/g_{cu})	average particle size (nm)
1	1.2	73	470	1.4
2	2.7	88	568	1.2
3	5.3	56	364	1.8
4	9.5	27	173	3.8
5	13.9	18	116	5.8
6	19.1	13	81	8.3

that the dispersion is maximum for 2.7 wt % of Cu on ZrO_2 and decreases with further increase of copper loading.

From the results of TPR and XRD, it is clear that larger β peak area of TPR (Figure 5) and larger signal intensity of CuO peaks in XRD (Figure 1) are observed with higher loadings of copper. There is a maximum area of α peak when the loading of Cu is 2.7 wt %. This further suggests that the β peak in TPR is due to copper oxide species belonging to the bulk CuO and the α peak to the dispersed CuO.

Copper dispersion (D_{Cu}), defined as the ratio of Cu exposed at the surface to total Cu present, was calculated from the amount of H_2 consumed in the s-TPR analysis. H_2 consumption (from s-TPR) can also be used to calculate the copper metal surface area (S_{Cu}) and the average particle size (ϕ_{av}) by means of the following assumptions and equations:

The area per copper surface atom in (100), (110), and (111) planes are 0.065, 0.092, and 0.056 nm^2, respectively.[50] An equal abundance of these three planes give an average copper surface atom area of 0.071 nm^2, equivalent to 1.4×10^{19} copper atoms per square meter. By assuming a spherical shape of the copper metal particles, S_{Cu} and ϕ_{av} can be expressed as eqs 1 and 2, respectively,

$$S_{Cu}\ (m^2\ g^{-1}{}_{Cu}) = Mol_{H2}\cdot SF\cdot N_A/(10^4\cdot C_M\cdot W_{Cu}) \quad (1)$$

$$\phi_{av}\ (nm) = 6000/(S_{Cu}\cdot \rho_{Cu}) \quad (2)$$

where Mol_{H2}, SF, N_A, C_M, W_{Cu}, and ρ_{Cu} are moles of hydrogen experimentally consumed per unit mass of catalyst ($\mu mol_{H2}\ g^{-1}{}_{cat}$), stoichiometric factor (2), Avogadro's number ($6.022 \times 10^{23}\ mol^{-1}$), number of surface Cu atoms per unit surface area, Cu content (wt %), and the density of copper (8.92 g cm^{-3}).[50]

The Cu percentage dispersion, metal surface area, and average particle size are given in Table 4. It was observed that the dispersion and metal area of copper are increased and average particle size is decreased up to 2.7 wt % of Cu on ZrO_2. This might be due to the maximum number of dispersed copper sites that are available on the catalyst surface. However, the dispersion and metal area are decreased, and average particle size is increased beyond this loading due to formation of CuO crystallites. This is also in good agreement with XRD and TPR.

The basicity measurements have been carried out by temperature-programmed desorption of CO_2 method. TPD of CO_2

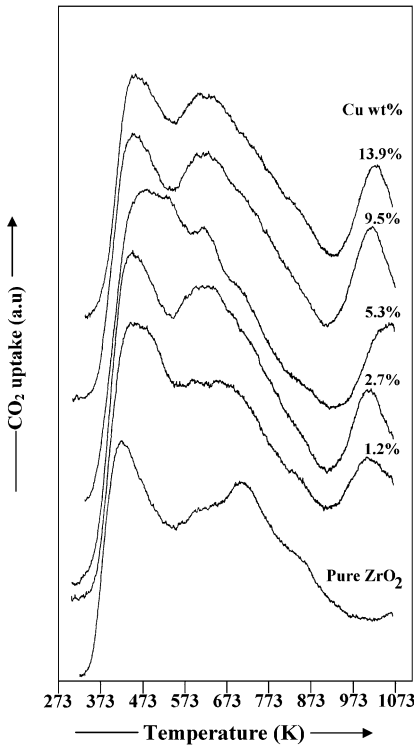

Figure 6. Temperature-programmed desorption of CO_2 profiles of various Cu/ZrO_2 catalysts.

TABLE 5: Temperature-Programmed Desorption of CO_2 of Various Cu/ZrO_2 Catalysts

sample	Cu loading (wt %)	CO_2 uptake[a] (μmol/g) A	B	C	total CO_2 uptake[a] (μmol/g)
1	0.0	136	247	−	383
2	1.2	161	253	74	488
3	2.7	166	517	88	771
4	5.3	225	260	77	562
5	9.5	127	262	78	467
6	13.9	121	252	68	441

[a] Calculated from temperature-programmed desorption of CO_2. A = due to weak basic sites. B = due to moderate basic sites. C = due to strong basic sites.

profiles of pure ZrO_2 and various Cu/ZrO_2 catalysts are shown in Figure 6. The desorbed peak of CO_2 was deconvoluted into three temperature regions, i.e., 330−500, 500−700, and >700 K correspond to weak, moderate, and strong basic sites, respectively.[51] The three peak areas were integrated and basic strengths are given in Table 5. In the case of pure ZrO_2 support, there are only two peaks corresponding to weak and moderate basic sites. However, the possibility that the desorption sites show continuous changes in desorption energy with the change in degree of surface coverage cannot be excluded. TPD of CO_2 results suggests that pure ZrO_2 is less basic when compared to Cu/ZrO_2 catalysts. Impregnation of CuO to ZrO_2 support facilitated the formation of strong basic sites that desorb CO_2 at higher temperatures. Such strong basic sites corresponding to desorption of CO_2 at higher temperatures were also mentioned over $MgO-ZrO_2$ and alkali modified CaO catalysts.[52,53] The number of basic sites with moderate and strong basic strengths was found to increase with Cu loading up to 2.7 wt % on zirconia and decreased with further loadings. The decrease in basicity at higher copper loadings might be due to the agglomeration of copper crystallites. This behavior is in good agreement with the catalytic activity, which decreases with increase of Cu loading beyond 2.7 wt % on zirconia. This clearly

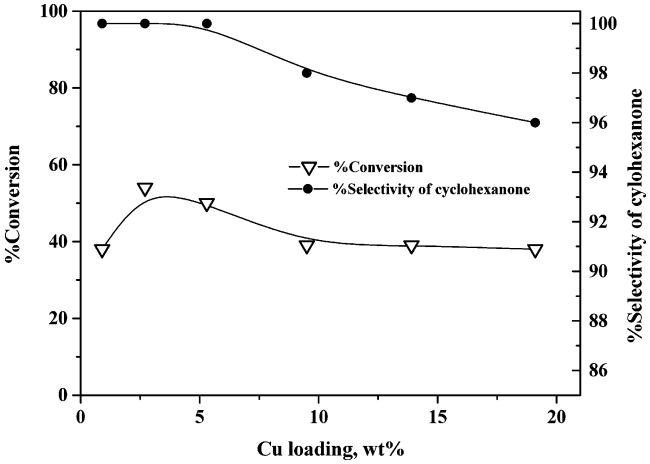

Figure 7. Dependence of dehydrogenation of cyclohexanol over various Cu/ZrO_2 catalysts.

indicates that moderate to strong basic sites are responsible for dehydrogenation of cyclohexanol.[54] The TPD results also suggest that the strength of basic sites plays a crucial role in determining the catalytic activity for dehydrogenation of cyclohexanol.

Figure 7 shows the dependence of activity and selectivity on copper loading for dehydrogenation of cyclohexanol to cyclohexanone at 523 K. The cyclohexanol conversion was found to increase with increase of Cu loading up to 2.7 wt % and decrease with further increase of copper loading on ZrO_2. The decrease in the catalytic activity of the catalysts beyond 2.7 wt % of Cu is due to increase of crystallinity of copper on the ZrO_2 support. The conversion of cyclohexanol for 1.2 wt % Cu loading catalyst was 38%, and it is increased to 54% when the copper loading is increased to 2.7 wt %. The medium and strong basic sites of the catalysts were also found to increase with copper loading up to 2.7 wt % and levels off at higher copper loadings. The selectivity toward cyclohexanone was independent of Cu loading. However, the selectivity toward cyclohexanone formation is slightly decreased at higher copper loadings. This might be due to increase in the crystallinity of Cu that makes more support surface for dehydration of cyclohexanol, resulting in the formation of cyclohexene due to weak acidic sites of the support. The bare support (pure ZrO_2) was found to be inactive for the cyclohexanone formation under the similar experimental conditions.

A comparison of the surface characterization and catalytic activity of 2.5 wt % of Cu supported on alumina, titania, niobia, and zirconia catalysts are reported in Table 6. The catalytic experiments were carried out under similar conditions for all the samples. The aim of this study is to assess the effect of the support on the catalytic properties in relation to surface properties such as dispersion, metal area, and basicity at approximately the same loading of copper. The results clearly show that copper is well dispersed on ZrO_2 support and also has higher copper metal area. The conversion of cyclohexanol is found to be higher in the case of the CuO/Al_2O_3 catalysts compared to those of the CuO/ZrO_2, CuO/Nb_2O_5, and CuO/TiO_2 catalysts. However, the selectivity towards cyclohexanone is found to be higher for CuO/ZrO_2 catalyst, when compared to other supported copper catalysts. This might be due to presence of more moderate and strong basic sites on CuO/ZrO_2 catalyst leading to dehydrogenation functionality during the vapor-phase dehydrogenation of cyclohexanol. The basic sites of all the samples have been measured by TPD of CO_2 and are reported in Table 6. Cyclohexene is the only byproduct formed

TABLE 6: Dispersion, Copper Metal Area, BET Surface Area, TPD of CO_2, and Dehydrogenation Activity Results of Various Supported Copper Catalysts

catalyst	dispersion[b] (%)	Cu metal[b] area (m^2/g_{cu})	CO_2 uptake[a] (μmol/g) A	B	C	conversion of cyclohexanol (%)	selectivity of cyclohexanone (%)
2.7% Cu/ZrO_2	88	568	166	517	88	54	100
2.5% Cu/Al_2O_3	67	433	407	882	−	58	03
2.5% Cu/Nb_2O_5	22	140	222	80	65	24	65
2.5% Cu/TiO_2	63	408	190	108	−	06	49

[a] Calculated from temperature-programmed desorption of CO_2. A = due to weak basic sites. B = due to moderate basic sites. C = due to strong basic sites. [b] Calculated from N_2O decomposition method.

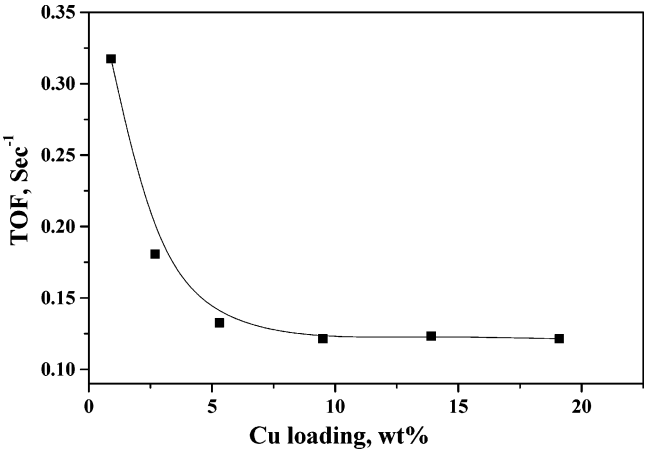

Figure 8. Relation between turnover frequency and copper loading.

during the vapor-phase dehydrogenation of cyclohexanol, and it is formed due to the acidic sites present on the support.

Carline et al.[55] reported similar observations in their study of the dehydrogenation/hydrogenation sites of various Cu/Mg−Al catalysts for the condensation of methanol with n-propanol to isobutyl alcohol and also compared the total amount of basic sites, percentage of medium, and strong basic sites of various metal supported catalysts. Manriquez et al.[54] have reported that strong acidic sites and weak basic sites are responsible for dehydration product, whereas dehydrogenation requires moderate acid sites and strong basic sites. The data given in Tables 5 and 6 are consistent with this assertion.

To find the relation between the dehydrogenation activity of cyclohexanol and the copper loading, a plot of turnover frequency (TOF) versus copper loading on ZrO_2 is shown in Figure 8, where TOF is defined as the number of cyclohexanol molecules converted per second per site of surface copper. The TOF was found to be constant for all the catalysts except for 1.2 and 2.7 wt % of Cu catalyst. This might be due to the presence of well-dispersed amorphous or isolated copper species at lower loadings, as shown from the TPR results.

4. Conclusions

Zirconia is found to be a good support material for supporting Cu for vapor-phase dehydrogenation of cyclohexanol to cyclohexanone. XRD results reveal the presence of crystalline CuO at high copper loadings (>2.7 wt %). N_2O decomposition is found to be a valuable method for measuring the dispersion of Cu on ZrO_2. The results of N_2O decomposition suggest that copper is found to be highly dispersed on the ZrO_2 support. The information obtained by UV−vis-DRS and TPR reveals the presence of two types of copper species on the ZrO_2 support. The dispersion of Cu as determined by N_2O decomposition substantiates the findings of XPS and XRD. TPD of CO_2 indicates the basicity of supported copper catalysts falls into three regions. Basicity of the catalysts was found to increase with increase of copper loading and decreases at higher loadings. The activity of the catalysts was found to increase up to 2.7 wt % and decreases at higher loadings in similar lines to copper dispersion and basicity measurements. CuO/ZrO_2 catalyst is found to be better than other supported copper catalysts under similar conditions.

Acknowledgment. G.V.S. thanks the Council of Scientific and Industrial Research (CSIR) for the award of a Senior Research Fellowship (SRF).

References and Notes

(1) Praliaud, H.; Mikhailenko, S.; Chajar, Z.; Primet, M. *Appl. Catal. B.* **1998**, *16*, 359.
(2) Radtke, F.; Koeppel, R. A.; Minardi, E. G.; Baiker, A. *J. Catal.* **1997**, *167*, 127.
(3) Agrell, J.; Birgersson H.; Boutonnet, M.; Melian-Cabrera, I.; Navarro, R. M. and Fierro, J. L. G. *J. Catal.* **2003**, *219*, 389.
(4) Kim T. W.; Song, M. W.; Koh H. L.; Kim, K. L. *Appl. Catal. A* **2001**, *210*, 35.
(5) Ma, Z-Y.; Yang, C.; Wei, W.; Li, W−H.; Sun, Y−H. *J. Mol. Catal. A* **2005**, *231*, 75.
(6) Saadi, A.; Rassoul, Z.; Bettahar, M. M. *J. Mol. Catal. A* **2000**, *164*, 205.
(7) Rao, R.; Dandekar, A.; Baker, R. T. K.; Vannice, M. A. *J. Catal.* **1997**, *171*, 406.
(8) Chary, K. V. R.; Sagar, G. V.; Naresh, D; Seela, K. K.; Sreedhar, B. *J. Phys. Chem. B* **2005**, *109*, 9437.
(9) Fabina, M. T.; Schmal, M. *Appl. Catal. A* **1997**, *163*, 153.
(10) Fridman, V. Z.; Davydov, A. A. *J. Catal.* **2000**, *195*, 20.
(11) Chen, K.; Xie, S.; Iglesia, E.; Bell, A. T. *J. Catal.* **2000**, *189*, 421.
(12) Ortelli, E. E.; Wambach, J.; Wokaun, A. *Appl. Catal. A* **2001**, *216*, 227.
(13) Tanabe, K.; Yamaguchi, T. *Catal. Today* **1994**, *20*, 185.
(14) Yamaguchi, T. *Catal. Today* **1994,** *20*, 199.
(15) Vrinat, M.; Hamon, D.; Breysse, M.; Durand, B.; Des Courrieres, T. *Catal. Today* **1994**, *20*, 273.
(16) Andersen, K. J.; Candia, R.; Rostrup-Neilsen, J. *Ger. Offen.* **1974**, *760*, 122.
(17) Andersen, K. J.; Candia, R.; Rostrup-Neilsen, J. *U.S. Patent* **1976**, *3,988*, 262.
(18) Lisitsyn, A. S.; Kuznetsov, V. L.; Yermakov, Y. I. *React. Kinet. Catal. Lett.* **1980**, *14*, 445.
(19) Brue, L. A.; Matthews, J. F. *Appl. Catal.* **1982**, *4*, 353.
(20) Bruce, L. A.; Hope, G. H.; Matthews, J. F. *Appl. Catal.***1983**, *8*, 349.
(21) Chang, C. D.; Perkins, P. D. *U.S. Patent* **1984**, *4,440*, 668
(22) Ichikawa, M. *Bull. Chem. Soc. Jpn.* **1978**, *51*, 2268.
(23) Miyata, H.; Tokuda, S.; Ono, T.; Ohno, T.; Hatayama, F. *J. Chem. Soc. Faraday Trans.* **1990**, *86*, 2291.
(24) Kulkarni D. and Waches, I. E. *Appl. Catal. A* **2002**, *237*, 121.
(25) Cubeiro M. L. and Fierro, J. L. G. *Appl. Catal. A* **1998**, *168*, 307.
(26) Burcham L. J. and Waches, I. E. *Catal. Today* **1999**, *49*, 467.
(27) Ilyas, M.; Ikramullah *Catal. Commun.* **2004**, *5*, 1.
(28) Koppel, R. A.; Stocker, C.; Baiker, A. *J. Catal.* **1998**, *179*, 515.
(29) Amenomiya, Y. *Appl. Catal.* **1987**, *30*, 57
(30) Takezawa, N.; Shimokawabe, M.; Hiramatsu, H.; Sugiura, H.; Asakawa H. and Kobayashi, H. *React. Kinet. Catal. Lett.* **1987**, *33*, 191.
(31) Velu, S.; Suzuki, K.; Okazaki, M.; Kapoor, M. P.; Osaki, T.; Ohashi, F. *J. Catal.* **2000**, *194*, 373.
(32) Iglesia, E.; Barton, D. G.; Soled, S. L.; Miseo, S.; Baumgartner, J. E.; Gates, W. E.; Fuentes, G. A.; Meitzner, G. D. *Stud. Surf. Sci. Catal.* **1996**, *101*, 533.
(33) Rijnten, H. Th. Ph.D Thesis, Delft Technical University, 1971.
(34) Afanaiev, P.; Geantet, F.; Breysse, M. *J. Catal.* **1995**, *153*, 17.

(35) Maity, S. K.; Rana, M. S.; Srinivas, B. N.; Bej, S. K.; Muralidhar, G.; Rao, T. S. R. P. *J. Mol. Catal. A.* **2000**, *153*, 121.
(36) Morterra, C.; Giamello, E.; Cerrato, G.; Centi, G.; Perathoner, S. *J. Catal.* **1998**, *179*, 111
(37) Praliaud, H.; Mikhailenko, S.; Chajar, Z.; Primet, M. *Appl. Catal. B* **1998**, *16*, 359.
(38) Praliaud, H.; Kodratoff, Y.; Coudurier, G.; Mathieu, M. V. *Spectrochim. Acta. Part A* **1974**, *30*, 1389.
(39) Iwamoto, M.; Yahiro, H.; Tanda, K.; Mizuno, Y.; Mine, Y.; Kagawa, S. *J. Phys. Chem.* **1991**, *95*, 3727.
(40) Mendes, F. M. T.; Schmal, M. *Appl. Catal. A* **1997**, *151*, 393.
(41) Bechara, R.; Aboukais, A.; Bonnelle, J-P. *J. Chem. Soc. Faraday Trans.* **1993**, *89*, 1257.
(42) Brigs, D., Seah, M. P., Eds.; *Practical Surface Analysis by Auger and X-ray Photoelectron Spectroscopy*; Wiley: New York, 1983.
(43) Chusuei, C. C.; Brookshier, M. A.; Goodman, D. W. *Langmuir* **1999**, *15*, 2806.
(44) Shimokawabe, M.; Asakawa, H.; Takezawa, N. *Appl. Catal.* **1990**, *59*, 45.
(45) Dow, W.; Wang, Y.; Huang, T. J. *J. Catal.* **1996**, *160*, 155.
(46) Robertson, S. D.; Minicol, B. D.; Debaos, J. H.; Kloet, S. C.; Jenkins, J. W. *J. Catal.* **1975**, *37*, 424.
(47) Vander Grift, C. J. G.; Mulder, A.; Geus, J. W. *Appl. Catal.* **1990**, *60*, 181.
(48) Gentry, S. J.; Walsh, P. T. *J. Chem. Soc. Faraday Trans. I* **1982**, *78*, 1515.
(49) Wollner, A.; Lange, F.; Schmeldz, H.; Knozinger, H. *Appl. Catal. A* **1993**, *94*, 181.
(50) Evans, J. W.; Wainwright, M. S.; Bridgewater, A. J.; Young, D. J. *Appl. Catal.* **1983**, *7*, 75.
(51) Diez, V. K.; Asperteguia, C. R.; Di Cosimo, J. I. *Catal. Today* **2000**, *63*, 53.
(52) Kabner, P.; Baerns, M. *Appl. Catal*. *A* **1996**, *139*, 107.
(53) Aramendia, M. A.; Borau, V.; Jimenez, C.; Marinas, A.; Marinas, J. M.; Ruiz, J. R.; Urbano, F. J. *J. Mol. Catal. A* **2004**, *218*, 81.
(54) Manriquez, M. E.; Lopez, T.; Gomez, R.; Navarrete, J. *J. Mol. Catal. A* **2004**, *220*, 229.
(55) Carline, C.; Marchionna, M.; Noviello, M.; Galletti, A. M. R.; Sbrana, G. Basile, F.; Vaccari, A. *J. Mol. Catal. A* **2005**, *232*, 13.